Environmental Science and Pollution Research
https://doi.org/10.1007/s11356-018-2266-x

RESEARCH ARTICLE

Migration and leaching characteristics of base cation: indicating environmental effects on soil alkalinity in a karst area

Mingzhen Ma[1,2] · Yang Gao[1,2] · Xianwei Song[1] · Sophie M. Green[3] · Bailian Xiong[4] · Jennifer A. J. Dungait[5] · Tao Peng[6] · Timothy A. Quine[3] · Xuefa Wen[1,2] · Nianpeng He[1,2]

Received: 17 December 2017 / Accepted: 7 May 2018

Abstract

In karst areas, rock dissolution often results in the development of underground networks, which act as subterranean pathways for rapid water and nutrient (and possibly soil) loss during precipitation events. Loss of soluble nutrients degrades surface soils and decreases net primary productivity, so it is important to establish flow pathways and quantify nutrient loss during rainfall events of different magnitudes. We conducted a simulated rainfall experiment in karst and nonkarst areas to compare the concentration of nutrients in surface and subsurface flow water and effects on soil alkalinity in three lithologic soil formations under five different rainfall intensity treatments. Compared with the nonkarst area, the runoff in subsurface flows and the proportion of nutrient loss in the subsurface flow are larger in the karst area and less affected by rain intensity. The maximum loss loads of calcium (Ca^{2+}) and magnesium (Mg^{2+}) ions were 32.9 and 19.8 kg ha^{-1}, respectively. With the estimate of base cation loss loads in the China southern karst area under the rainfall intensity of 45 mm h^{-1}, more than 80% of the base cation loss load occurred in the limestone karst area. Although the alkalinity leaching value in nonkarst was similar to that in the karst area under simulated rainfall conditions, its impact on the ecological environment was quite different.

Keywords Karst · Lithologic · Simulated rainfall · Base cations · Soil degradation · Solute transport

Introduction

Karst covers approximately 22 million km^2 globally, which equates to 15% of the total land surface area on Earth. In China, the karst area occupies approximately 3.6 million km^2 (1% of the country's total land area) (Fig. 1), with rocky desertification (rocky outcrops) accounting for approximately 1.3 million km^2. China's southwestern karst area is "the world's largest karst continuous belt" (Tuyet 2001; Chen et al. 2013), with a total area of 540,000 km^2 (Cai 1996) and with Guizhou Province accounting for 61.9% of the province's land area (Zhang et al. 2001). The stability and resilience of karst ecosystems is very low and extremely fragile. In karst areas, there is often no weathered parent transition layer between the bedrock interface and the soil due to erosion, which leads to poor water storage capacity and propagates further loss of soil (Xiao and Weng 2007).

Karst areas are characterized by low soil formation rate (Sweeting 1993; Zhang et al. 2001) and large potential for soil erosion and ultimately bedrock exposure (rocky desertification) (Yuan 1997). Furthermore, strong dissolution leads to the development of complex underground structures where fissures, funnels, and sinkholes promote rapid water loss during and after rainfall (Peng et al. 2017; Yi et al. 2012). Subsurface flows are the primary means of macronutrient loss

Responsible editor: Zhihong Xu

✉ Yang Gao
gaoyang@igsnrr.ac.cn

[1] Key Laboratory of Ecosystem Network Observation and Modeling, Institute of Geographic Sciences and Natural Resources Research, CAS, Beijing 100101, People's Republic of China

[2] College of Resources and Environment, University of Chinese Academy of Sciences, Beijing 100190, People's Republic of China

[3] Geography, Amory Building, University of Exeter, Rennes Drive, Exeter EX4 4RJ, UK

[4] College of Resources and Environment, Zunyi Normal College, Zunyi 563002, People's Republic of China

[5] Department of Sustainable Soils and Grassland Systems, Rothamsted Research, North Wyke, Okehampton EX20 2SB, UK

[6] State Key Laboratory of Geochemistry, Geochemistry Institute of CAS, Guiyang, Guizhou 550002, People's Republic of China

Published online: 15 May 2018

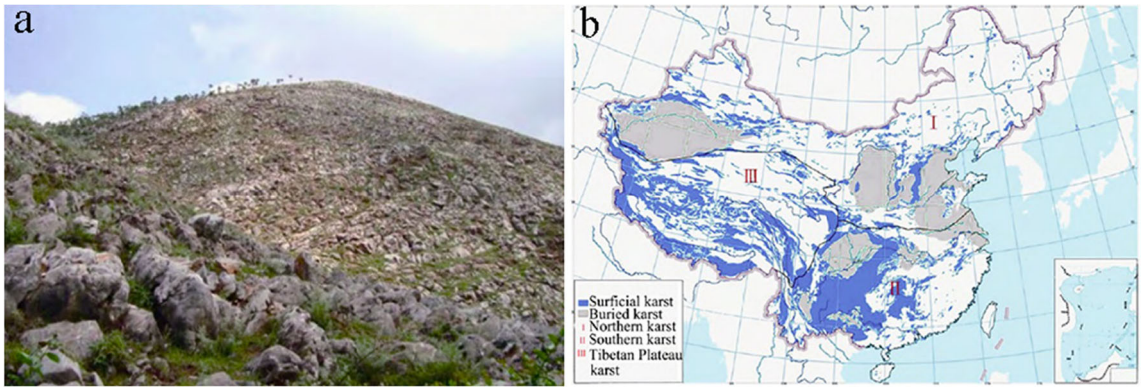

Fig. 1 **a** Rocky desertification caused by soil erosion in the karst area. **b** China karst landform distribution (Song et al. 2017a)

in the karst areas: the ratio of total nitrogen (TN), total phosphorus (TP), and total potassium (TK) output loads in subsurface flow is higher than 46.70% (Peng et al. 2017). However, base cations in water in surface and subsurface flow under different rainfall intensities and in different lithologies have not been systematically studied.

Base cations (calcium (Ca^{2+}), magnesium (Mg^{2+}), potassium (K^+), and sodium (Na^+)) are the predominant exchangeable ions in calcareous soils (Xu et al. 2013) and control cation exchange capacity (CEC), a key indicator of soil quality (Huang et al. 2016). Losses of base cations from soil by leaching (Liu et al. 2008; Watmough and Dillon 2004) drive soil acidification (Cronan and Grigal 1995; Wang and Dai 2012). Moreover, ions critical for net primary productivity (NPP) are lost (Cheng et al. 2010) affecting key physiological processes, e.g., photosynthesis (K^+, Mg^{2+}), photorespiration (K^+), osmotic regulation of cells and water use efficiency (Na^+), and plant tissue morphology and plant cell signaling (Ca^{2+}) (Gattward et al. 2012; Liang et al. 2009; Lucas et al. 2011; Pettigrew 2008; Powers and Salute 2011; Wang et al. 2004). In addition, the absence of Mg^{2+} stimulates microbial decomposition of litter (Powers and Salute 2011), leading to an increase of the leaching of soluble minerals into the soil.

There are also implications for surface and subsurface water quality as the nutrients leached into the surrounding water bodies lead to an increase in water hardness and salinity, impacting aquatic organisms (Silva et al. 2003), e.g., high Ca^{2+} and Mg^{2+} slow down the growth rate of fish (Wang and Zhang 2010), and human health, such as gastrointestinal discomfort, kidney stones, and cerebrovascular diseases (Tang et al. 2014). Despite the vulnerability of karst ecosystems to soil degradation and loss, and the importance of base cations to ecosystem and human health, the effects of different rainfall intensities on base cation dynamics are rarely studied.

In this paper, we explored the relationship between rainfall and cation loss in karst systems by testing two hypotheses: (1) due to the developed underground structures in the karst area, water and BC (summed base cations = $Ca^{2+} + K^+ + Mg^{2+} + Na^+$) loss in subsurface flow will be very different from the nonkarst area, and the proportions of water and BC in subsurface flow will be less affected by rain intensity and higher in the karst area than the nonkarst area; and (2) migration and leaching characteristics of base cations will be significantly influenced by the chemical composition of the parent bedrocks, and there will be more Mg^{2+} loss in dolomite karst area (chemical formula $CaMg(CO_3)_2$) and more Ca^{2+} loss in limestone karst area (chemical formula $CaCO_3$). To address these hypotheses, we selected three different lithologic soil formations (two karst soils, dolomite and limestone, and one nonkarst soil) in Guizhou Province and conducted simulated rainfall experiments.

Materials and methods

Study area

Three experimental sites were established in Shawan (SW), Chenqi (CQ), and Huangtupo (HTP), all of which are located within Puding County (26° 15′ N, 105° 43′ E) (Fig. 2a), Guizhou Province, China, with the altitude of 1042–1846 m. The three experimental sites were within 14 km and have similar climates. They are all within the subtropical monsoon humid climate zone, where the average annual temperature is 15.1 °C and the average annual rainfall is 1336.0 mm (Zheng et al. 2014). SW and CQ represent two different typical karst zones (developed from dolomite and limestone, respectively), with an approx. mean soil depth of 0.60 m. HTP (nonkarst) served as the experimental control site and had a mean soil depth in excess of 1.50 m. Soils from these three sites underwent different lithologic developmental processes. Both SW and CQ sites are grassland, while HTP is nonvegetated. Table 1 provides the soil basic physical and chemical properties associated with each site (Song et al. 2017a).

Experimental design of simulated rainfall

Three replicate rainfall plots (Fig. 2b) at each site were established in June 2016, which were 1.7 m long and 1.2 m

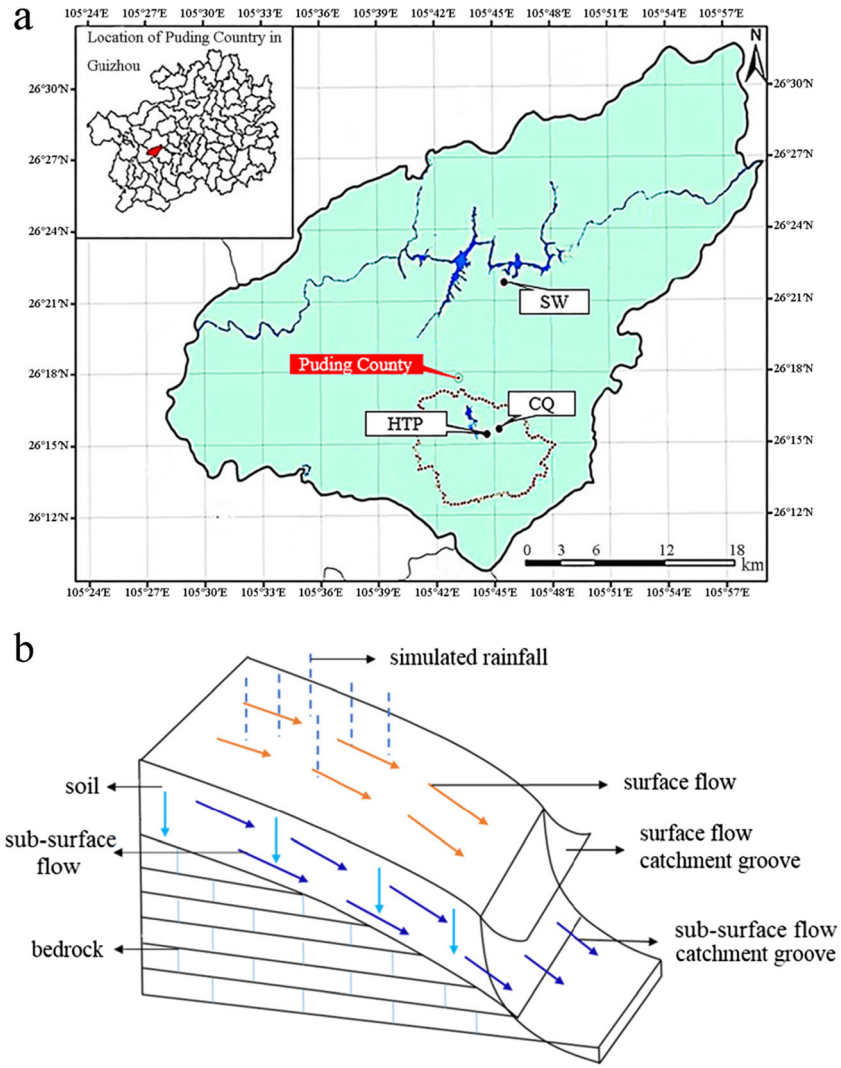

Fig. 2 **a** Geographic location of the experimental sites. **b** Schematic of simulated rainfall

wide at a gradient from approximately 12° to 20°. The area of effective rainfall was 1.9 m^2. All four sides of the plots were dug into the bedrock with an average approximate depth from 0.5 to 0.7 m. They were then secured with concrete. The catchment grooves used for surface flow and subsurface flow were coated with high molecular polymer, cement, and quartz powder. We connected a conduit to the catchment grooves, which could be used to introduce rainfall into plastic buckets. Rainfall brackets were surrounded by absorbent flannel to insulate from wind effects as well as rainwater secondary sputtering into plots at the nozzles. We covered the area surrounding the plots with tarpaulin to prevent rainwater seepage from the edge of the plots into the subsurface flow catchments.

We used the NLJY-10 small-scale field-simulated rainfall device (Nanjing Electronic Technology Co., Ltd., Nanjing City, China). The "down jet type" was used as the rainfall pattern. Rainfall height was 3 m and the rainfall uniformity coefficient > 0.86. Based on the eroded rainfall intensity in Guizhou karst area (about 10 to 50 mm h^{-1} rainfall) (Zhang et al. 2014a; Yang et al. 2010), five rainfall intensities were selected: 30, 45, 70, 90, and 120 mm h^{-1}. Rainfall time was set at 60 min. We monitored real-time rainfall intensity using a rain gauge to ensure uniform and stable rainfall intensities. The initial runoff yield times were recorded after the start of the simulated rainfall treatments. After each rainfall experiment, we measured the volume (L) of all water collected in the plastic buckets as the runoff of surface and subsurface flow, and sampled 100 mL of the mixed rainwater from the plastic buckets to prepare for testing.

Water analysis method

Water was filtered through a 0.45-μm organic microporous membrane (Shanghai Binlon Instrument Co. Ltd., China) (treated in an 80 °C water bath for 8 h). Alkalinity was measured by using the Photometer 7500 (Palintest Ltd., UK). The concentrations of base cations (Ca^{2+}, K^+, Mg^{2+}, Na^+) were measured by using an Optima 5300 DV ICP-OES

Table 1 Basic physical and chemical properties of soils from the three experimental sites

Site	Soil type	pH	Bulk density (N m^{-3})	Porosity (%)	Particle size			Conductivity (μS cm^{-1})	TN (g kg^{-1})	TC (g kg^{-1})
					< 0.002 mm	0.002–0.02 mm	> 0.02 mm			
SW	Lime soil	7.86	1.53	43.5	10.4	69.9	19.8	180.0	0.28	6.96
CQ	Lime soil	7.66	1.28	51.7	15.1	74.5	10.4	143.6	0.32	4.09
HTP	Mixed of red and yellow soil (red-yellow soil)	7.82	1.17	55.3	14.0	69.8	16.2	138.9	0.16	1.98

Inductively Coupled Plasma Spectrometer (PerkinElmer, Inc., MA, USA). The simulated rainfall was used as a blank control, and the differences between actual measured values and blank control values are the ultimate loss values.

Statistical analysis

We used SPSS 22.0 (IBM Ltd., USA) to analyze the significance and relevance of the data, and used the Origin 9.0 to draw charts. In order to test the hypotheses posed, the proportions of runoff in subsurface flow in the three sites were calculated with the total runoff of surface flow and subsurface flow divided by the runoff of subsurface flow; the calculation of the proportions of BC in subsurface flow was the same as the runoff. Then, one-way ANOVA was performed for analysis of variance of the proportions of water in subsurface flow in three different sites as well as the proportions of base cations in subsurface flow. If the value of p is less than 0.05, that means there is a significant difference between two sites. Then, the assumption of difference of the proportions of runoff and BC in subsurface flow between the karst area and nonkarst area would be tested. The calculation of base cations loss loads in experimental sites is cation concentration multiplied by runoff in surface/subsurface flow. The histograms of base cations' loss concentrations and the table of loss loads were made to intuitively test the hypotheses of the effect of bedrocks to base cations' migration characteristics.

Pearson test was used to describe the correlation level between rainfall intensity and all indexes.

Estimated method

According to the China southern karst area (II) distribution (Song et al. 2017a) (Fig. 1), dolomite and limestone distribution proportions, and annual average rainfall during the period of 1961–2014 in China southern karst area (Song et al. 2017b), the following formulas (1), (2), and (3) were used to estimate annual average loss load of base cations from karst soil in the China southern karst area:

$$L_i = a \times S \times Q \times c_{ai} + b \times S \times Q \times c_{bi} \quad (1)$$

$$Q = R \times C \quad (2)$$

$$C = \frac{Q_S}{R_S} \quad (3)$$

where L is the loss load (Tg a^{-1}); i represents base cations (i = Ca^{2+}, K^+, Mg^{2+}, Na^+); a is the proportion of the dolomite karst area and b is the proportion of the limestone karst area in the China southern karst area ($a = 0.2$, $b = 0.8$); S is the China southern karst area (km^2) (the value is 127.5×10^4 km^2); Q is the runoff depth (mm); c_a is the loss concentration of base cation in the dolomite karst area; c_b is the loss concentration of

base cation in the limestone karst area; R is the annual average rainfall (1359 mm); C is the runoff coefficient; Q_S is the runoff depth in the simulated rainfall experiment (mm), and the value is equal to runoff per unit area; and R_S is the rainfall per unit hour in the simulated rainfall experiment (mm), and the value is equal to rainfall intensity.

In addition, we evaluated the critical soil alkalinity leaching potential. Based on the charge balance of ions in the soil solution, soil (karst ecosystem) acid-base balance, soil stability critical alkalinity leaching potential was derived using Expression (4) (Sverdrup and Vries 1994; Duan et al. 2000, 2002):

$$\mathrm{ALK_{L,crit}} = -\mathrm{r}\cdot \mathrm{BC}_W - Q^{\frac{2}{3}}\cdot\left[\frac{r\cdot \mathrm{BC}_W}{K_{gibb}}\right]^{\frac{1}{3}} \quad (4)$$

where ALK is alkalinity, defined as the sum of the base cations in the solution subtracted by the sum of strong acid anions (in $\mathrm{keq\cdot ha^{-1}\cdot a^{-1}}$, corresponding to $\mathrm{kmol\cdot ha^{-1}\cdot a^{-1}}$ in the International System of Units); subscript L indicates leaching and crit indicates the critical value; r is the equivalent ratio of Al^{3+} to base cations produced by primary mineral weathering ($r = 2$ is the typical value); BC_W is the sum of the base cations produced by mineral weathering ($BC = Ca^{2+} + Mg^{2+} + K^{+} + Na^{+}$), estimated according to the typical soil mineral type (in $\mathrm{keq\cdot ha^{-1}\cdot a^{-1}}$) ($BC_W$ values of lime soil and red-yellow soil are 1.02 and 0.16 $\mathrm{keq\cdot ha^{-1}\cdot a^{-1}}$, respectively); Q is the remaining precipitation (in $\mathrm{m^3\cdot ha^{-1}\cdot a^{-1}}$), which is the residual amount of precipitation subtracted by canopy interception evaporation and actual water evaporation of soil and roots, typically replaced by runoff; and K_{gibb} is the equilibrium constant of gibbsite, whose value is related to soil type (in $\mathrm{m^6\cdot eq^{-2}}$) ($K_{gibb}$ value of lime soil and red-yellow soil is 950 $\mathrm{m^6\ eq^{-2}}$).

Results and analysis

Characteristics of runoff

Under the simulated rainfall treatments, initial runoff yield times decreased with increasing rainfall intensity ($p < 0.05$) (Fig. 3a–c). When rainfall intensity was greater than 70 mm $\mathrm{h^{-1}}$, initial runoff yield times stabilized and changed from 0.4 to 9.7 min. This demonstrated that in the three experimental sites, the characteristic rainfall intensity of runoff was 70 mm $\mathrm{h^{-1}}$. For the rainfall treatments below this threshold (70 mm $\mathrm{h^{-1}}$), the rainfall convergence rate significantly increased with an increase in rainfall intensity, and initial runoff yield times significantly decreased. Under the 30-mm-$\mathrm{h^{-1}}$ rainfall intensity treatment, we observed no surface flow in all three sites, and the value of initial runoff yield times of subsurface flow was HTP > CQ > SW. However, under the 45-mm-$\mathrm{h^{-1}}$ rainfall intensity treatment, initial runoff yield times of surface flow and subsurface flow in HTP were significantly lower compared to those in CQ and SW. Under the most intense rain treatment (120 mm $\mathrm{h^{-1}}$), there were no statistical differences between initial runoff yield times of surface flow and subsurface flow between all three sites.

Rain intensity had a significant effect on runoff ($p < 0.01$) (Fig. 3d–f). The greatest change of runoff per unit area in surface flow occurred in HTP under an increase in rainfall intensity. When rainfall intensity increased from 45 to 120 mm $\mathrm{h^{-1}}$, runoff increased by a factor of 57.6 in HTP, while smaller variations of runoff per unit area in surface flow were observed in SW and CQ, with increases by a factor of 9.5 and 6.2, respectively. When rainfall intensity was 30 mm $\mathrm{h^{-1}}$, the runoff per unit area in subsurface flow was less than 5 L in CQ

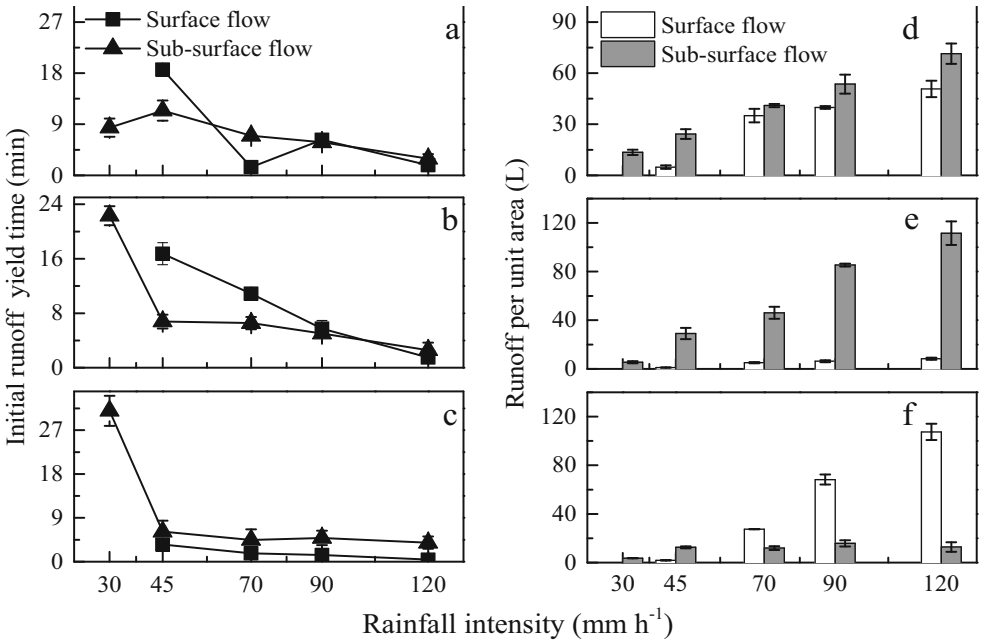

Fig. 3 Changes in initial runoff yield times and runoff per unit area for **a**, **d** SW; **b**, **e** CQ; and **c**, **f** HTP under the different rainfall intensities

and HTP, while the value in SW was greater than 12 L. With an increase in rainfall intensity, there were significant increases in runoff per unit area in both surface flow and subsurface flow in SW ($p < 0.01$). The increase in subsurface flow was more obvious compared to surface flow in CQ. Contrary to CQ, there was a greater increase in runoff per unit area in surface flow compared to subsurface flow in HTP.

With an increase in rain intensity, changes in the proportions of water in subsurface flow were small in SW and CQ (the karst area), while the proportions of water in subsurface flow in HTP (the nonkarst area) significantly reduced. Moreover, the proportions of water loss in subsurface flow in the karst area were significantly higher than those in the nonkarst area (SW > CQ > HTP, $p < 0.05$), while, under all five rainfall intensities, the proportions of water loss in subsurface flow were larger than 90% in CQ and 50% in SW.

Changes in base cation concentration losses in surface flow

$[Ca^{2+}]$ losses in surface flow increased in HTP with an increase in rainfall intensity, initially decreased before increasing in SW, and initially increased before decreasing in CQ (Fig. 4a). Losses in $[K^+]$ in surface flow in all three sites decreased with an increase in rainfall intensity (Fig. 4b). Losses in $[Mg^{2+}]$ in SW surface flow were greater compared to those in CQ and HTP for all four rainfall treatments, but such losses were lower with an increase in rainfall intensity, with concentrations ranging from 21.6 to 24.0 mg L^{-1} (Fig. 4c). Losses in $[Mg^{2+}]$ in surface flow first increased before decreasing with an increase in rainfall intensity in CQ and increased with an increase in rainfall intensity in HTP. Comparing Fig. 4b and d, changes in $[Na^+]$ loss in surface flow were similar to $[K^+]$, and these losses decreased with an increase in rainfall intensity.

In general, losses in $[Ca^{2+}]$ and $[Mg^{2+}]$ in SW surface flow were greater compared to those in CQ and HTP. When rainfall intensity was low (45 mm h^{-1}), losses in $[K^+]$ and $[Na^+]$ in surface flow were high in CQ and HTP. Losses in $[Ca^{2+}]$ and $[Mg^{2+}]$ in surface flow had no obvious regularity with increases in rainfall intensity, while losses in $[K^+]$ and $[Na^+]$ decreased with an increase in rainfall intensity.

Changes in base cation concentration losses in subsurface flow

Losses in $[Ca^{2+}]$ in subsurface flow first increased before decreasing with an increase in rainfall intensity in SW, exhibited a slight change in HTP, but exhibited a more pronounced change and irregularly in CQ compared to the other two sites (Fig. 5a). Losses in $[K^+]$ in SW subsurface flow first decreased before increasing and then decreasing once again with an increase in rainfall intensity, decreased with an increase in rainfall intensity in CQ, and first decreased before increasing in HTP (Fig. 5b). The maximum $[K^+]$ loss in HTP subsurface flow was 63.4 mg L^{-1} under the 30-mm-h^{-1} rainfall intensity treatment. Similar to surface flow, losses in $[Mg^{2+}]$ in SW subsurface flow were at all times greater compared to those in CQ and HTP for all five rainfall intensity treatments (Fig. 5c). Losses in $[Mg^{2+}]$ in subsurface flow changed only slightly in CQ, with values ranging from 7.5 to 11.2 mg L^{-1}. Changes in $[Mg^{2+}]$ losses in HTP subsurface flow were identical to those in SW, while the range of change was greater compared to that in SW. $[Na^+]$ losses in SW decreased with an increase in rainfall intensity, while corresponding losses in CQ and HTP first increased before decreasing (Fig. 5d). Under the 30-mm-h^{-1} rainfall intensity treatment, losses in subsurface flow $[Na^+]$ in CQ were significantly higher compared to those in SW and HTP.

In addition, with the increase in rain intensity, changes in the proportions of summed BC in subsurface flow were small in SW and CQ (the karst area), while the proportions of BC in subsurface flow in HTP (the nonkarst area) significantly reduced. Moreover, the proportions of BC loss in subsurface

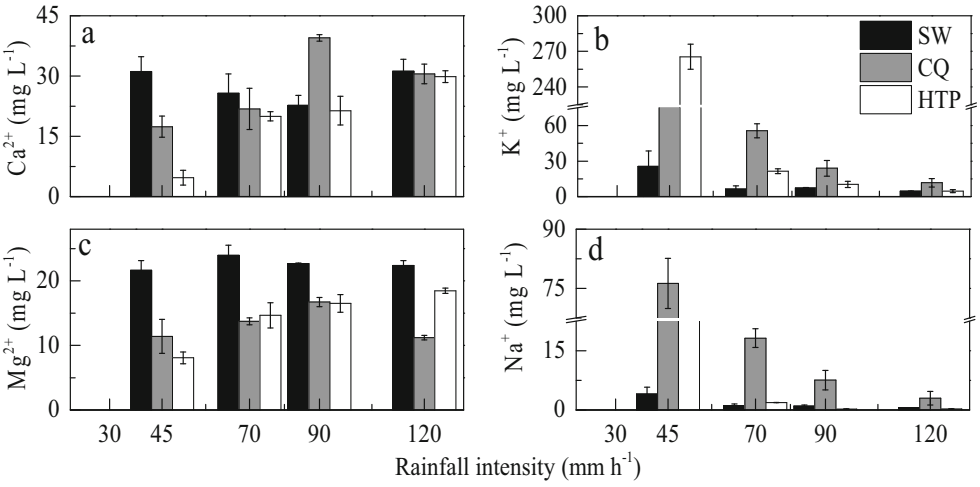

Fig. 4 Changes in **a** $[Ca^{2+}]$, **b** $[K^+]$, **c** $[Mg^{2+}]$, and **d** $[Na^+]$ losses (mg L^{-1}) in surface flow under the different rainfall intensities

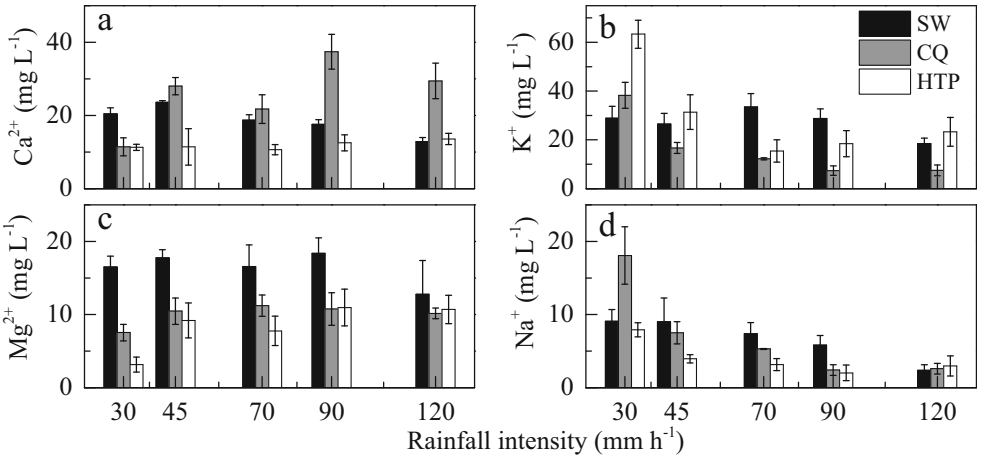

Fig. 5 Changes in **a** [Ca^{2+}], **b** [K^{+}], **c** [Mg^{2+}], and **d** [Na^{+}] losses (mg L^{-1}) in subsurface flow under the different rainfall intensities

flow in the karst area are significantly higher than those in the nonkarst area (SW > CQ > HTP, $p < 0.05$).

Correlations between rainfall intensity and base cation concentration losses

Significant positive correlations were observed between rainfall intensity and [Ca^{2+}] and [Mg^{2+}], while [K^{+}] and [Na^{+}] were negatively correlated with rainfall intensity (Table 2). In addition, there were strong connections between [Ca^{2+}] and [Mg^{2+}] and between [K^{+}] and [Na^{+}], wherein Pearson correlation coefficients were $r = 0.677$ ($p < 0.01$) and $r = 0.804$ ($p < 0.01$), respectively (Table 2). Losses in [Ca^{2+}] and [Mg^{2+}] in surface flow in HTP showed a strong positive correlation with the rain intensity, and the correlation intensity in SW and CQ was less than that in HTP (Table 3). There was a strong negative correlation between [Na^{+}] and rain intensity in subsurface flow in the three experimental sites. The nature and intensity of the impacts of rain intensity on the base cation concentration losses in different sites are different.

Migration characteristics of base ions for the different lithologic soil formations and rainfall intensity treatments

Ca^{2+} and Mg^{2+} loss loads from SW and CQ in surface flow and subsurface flow generally increased with an increase in rainfall intensity, but only Ca^{2+} and Mg^{2+} loss loads from surface flow in HTP exhibited the corresponding behavior (Table 4). The loss load of K^{+} and Na^{+} did not show those clear regular patterns as Ca^{2+} and Mg^{2+} in all three sites.

Under the five rainfall intensities investigated, the proportion of Ca^{2+}, Mg^{2+}, and K^{+} + Na^{+} in SW was predominantly between 25 and 50%, while the proportion of Ca^{2+} and K^{+} + Na^{+} loss in CQ and the proportion of Ca^{2+}, Mg^{2+}, and K^{+} + Na^{+} loss in HTP were both greatly affected by changes in rainfall intensity. With an increase in rainfall intensity, the proportion of Ca^{2+} and Mg^{2+} in SW showed an increasing trend, and the proportion of K^{+} + Na^{+} showed a decreasing trend (Fig. 6a). In CQ (Fig. 6b), the proportion of Ca^{2+} increased with an increase in rainfall intensity, the proportion of K^{+} + Na^{+} decreased, and the proportion of Mg^{2+} slowly increased. Changes in base cation loss proportions in HTP (Fig. 6c) corresponded to those in SW. Under low rainfall intensity, base cation losses in the karst area were mainly in the form of K^{+} + Na^{+}, while the proportion of Ca^{2+} and Mg^{2+} was greater under the heavy rainfall intensity.

In order to explore allocation of base cation loss loads in the dolomite and limestone karst area, we selected the loss concentration of base cations under the rainfall intensity of 45 mm h^{-1} combined with the annual average rainfall data of 1961–2014 to estimate annual average loss loads of base cations in the China southern karst area

Table 2 Correlation analysis between rainfall intensity and [Ca^{2+}], [K^{+}], [Mg^{2+}], and [Na^{+}] loss (mg L^{-1})

Rainfall intensity		Ca^{2+}	K^{+}	Mg^{2+}	Na^{+}
Rainfall intensity	1	0.508**	−0.277**	0.439**	−0.286**
Ca^{2+}	0.508**	1	−0.227*	0.677**	−0.089
K^{+}	−0.277**	−0.227*	1	−0.116	0.804**
Mg^{2+}	0.439**	0.677**	−0.116	1	−0.067
Na^{+}	−0.286**	−0.089	0.804**	−0.067	1

* and ** indicate significant level at $p < 0.05$ and 0.01, respectively

Table 3 Correlation analysis between rainfall intensity and [Ca^{2+}], [Mg^{2+}], [K^+], and [Na^+] loss (mg L^{-1})

Site		Ca^{2+}	K^+	Mg^{2+}	Na^+
SW	Surface flow	0.594*	− 0.192	0.644**	− 0.247
	Subsurface flow	− 0.859**	− 0.466	− 0.378	− 0.827**
CQ	Surface flow	0.821**	− 0.359	0.604*	− 0.376
	Subsurface flow	0.633*	− 0.805**	0.377	− 0.803**
HTP	Surface flow	0.962**	− 0.395	0.912**	− 0.402
	Subsurface flow	0.348	− 0.673**	0.676**	− 0.696**

* and ** indicate significant level at $p < 0.05$ and 0.01, respectively

(Table 5). Base cation loss load in the limestone karst area accounted for 80% of the total loss load in the southern karst region. In general, loss loads of Ca^{2+} and K^+ were far higher than those of Mg^{2+} and Na^+.

Alkalinity leaching in different lithologic soil formations

Alkalinity leaching in surface flow and subsurface flow in both SW and CQ under the five types of rainfall intensities exceeded the critical threshold, indicating that loss of BC by rainfall might lead to soil acidification in both areas (Fig. 7). The alkalinity leaching values were not significantly different under rainfall intensity treatments for the three lithologic soil formations, most being between − 1.5 and 0 keq ha^{-1} a^{-1}, but due to the different critical alkalinity leaching values of the different soil types, alkalinity leaching resulting from rainfall had significantly different impacts on soil properties and ecological environments for the three lithologic soil formations investigated.

The critical alkalinity leaching value of lime soil (karst area) was small, only − 2.16 keq ha^{-1} a^{-1}, and alkalinity leaching in SW and CQ under the simulated rainfall treatments

Table 4 Loss loads of base cations under the different simulated rainfall treatments

Site	Rainfall intensity (mm h^{-1})		Loss load (kg ha^{-1})			
			Ca^{2+}	K^+	Mg^{2+}	Na^+
SW	Surface flow	30				
		45	0.35 ± 0.15	1.16 ± 0.46	1.06 ± 0.29	0.19 ± 0.06
		70	1.24 ± 0.26	2.30 ± 1.23	8.35 ± 0.43	0.38 ± 0.21
		90	7.90 ± 0.09	2.90 ± 0.13	9.02 ± 0.21	0.39 ± 0.10
		120	12.44 ± 1.36	2.32 ± 0.24	11.35 ± 1.08	0.27 ± 0.03
	Subsurfac flow	30	2.74 ± 0.11	3.93 ± 1.11	2.22 ± 0.31	1.21 ± 0.09
		45	5.73 ± 0.66	6.36 ± 0.42	4.30 ± 0.37	2.17 ± 0.77
		70	7.65 ± 0.44	13.71 ± 2.13	6.80 ± 1.33	3.02 ± 0.57
		90	9.40 ± 1.08	15.43 ± 2.74	9.82 ± 1.36	3.12 ± 0.69
		120	9.23 ± 1.54	13.13 ± 0.45	8.94 ± 2.51	1.67 ± 0.40
CQ	Surface flow	30				
		45	0.11 ± 0.02	2.35 ± 0.32	0.13 ± 0.04	0.89 ± 0.06
		70	0.26 ± 0.07	2.81 ± 0.11	0.70 ± 0.08	0.92 ± 0.09
		90	2.01 ± 0.18	1.53 ± 0.59	1.04 ± 0.11	0.48 ± 0.19
		120	1.91 ± 0.33	0.96 ± 0.22	0.94 ± 0.13	0.24 ± 0.12
	Subsurface flow	30	0.64 ± 0.24	2.13 ± 0.55	0.41 ± 0.00	0.99 ± 0.20
		45	8.19 ± 1.68	4.92 ± 1.47	3.08 ± 0.93	2.23 ± 0.83
		70	10.06 ± 2.40	5.65 ± 0.76	5.20 ± 1.10	2.45 ± 0.29
		90	31.99 ± 4.47	6.32 ± 1.74	9.19 ± 2.02	2.07 ± 0.63
		120	32.86 ± 6.50	8.26 ± 2.05	11.28 ± 0.50	2.90 ± 0.77
HTP	Surface flow	30				
		45	0.02 ± 0.01	4.87 ± 0.59	0.15 ± 0.03	0.55 ± 0.14
		70	0.37 ± 0.07	5.92 ± 0.55	4.03 ± 0.55	0.52 ± 0.00
		90	5.88 ± 0.96	7.05 ± 1.96	11.27 ± 1.22	0.16 ± 0.02
		120	20.35 ± 0.39	4.95 ± 1.12	19.84 ± 1.10	0.28 ± 0.02
	Subsurface flow	30	0.41 ± 0.02	2.31 ± 0.13	0.12 ± 0.04	0.29 ± 0.03
		45	1.42 ± 0.56	3.99 ± 1.17	1.15 ± 0.25	0.50 ± 0.09
		70	1.29 ± 0.34	1.83 ± 0.49	0.93 ± 0.28	0.39 ± 0.15
		90	1.98 ± 0.45	2.82 ± 0.34	1.78 ± 0.65	0.30 ± 0.10
		120	1.75 ± 0.60	2.84 ± 0.31	1.41 ± 0.61	0.35 ± 0.03

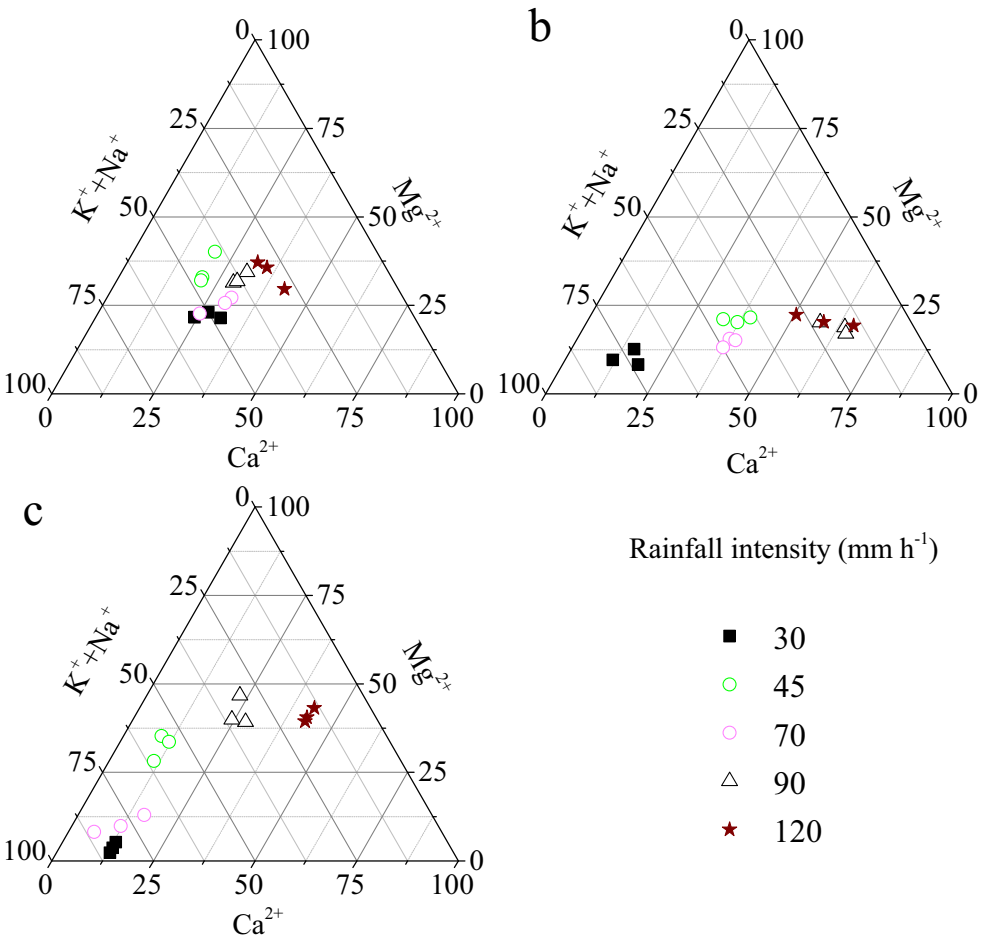

Fig. 6 Proportional changes of base cations in **a** SW, **b** CQ, and **c** HTP under the different rainfall intensities

exceeded their critical values. In the HTP (nonkarst), the critical alkalinity leaching value was relatively high (−0.38 keq ha^{-1} a^{-1}), and the alkalinity leaching value in the experiment was lower than its critical value under different rainfall intensities in subsurface flow, but it exceeded that critical value in surface flow. Thus, soil was at risk for acidification in the karst area under simulated rainfall conditions.

In addition, the alkalinity of the two routes was not very different in SW and CQ, while the alkalinity loss in surface flow was significantly greater than that in subsurface flow in HTP. That means that surface flow is the main way of soil alkalinity leaching in the nonkarst area.

Discussion

Effects of rainfall intensity and lithology on runoff characteristics

The initial runoff yield time is the time from the beginning of rainfall to the occurrence of runoff in the catchment groove, which is an important indicator of soil erosion (Qian et al. 2014). The effect of rainfall intensity on initial runoff yield times and runoff was mainly due to precipitation and the kinetic energy of raindrops on soil surface erosion, which affected the infiltration rate of water and precipitation distribution

Table 5 Annual average loss load of base cations in China southern karst area (Tg a^{-1})

	Dolomite			Limestone		
	Surface flow	Subsurface flow	Total	Surface flow	Subsurface flow	Total
Ca^{2+}	1.19	4.42	5.61	0.72	24.87	25.59
K^+	0.97	4.96	5.93	8.37	14.79	23.16
Mg^{2+}	0.82	3.33	4.15	0.47	9.29	9.76
Na^+	0.15	1.69	1.84	3.17	6.66	9.83
Total	3.14	14.40	17.54	12.74	55.61	68.36

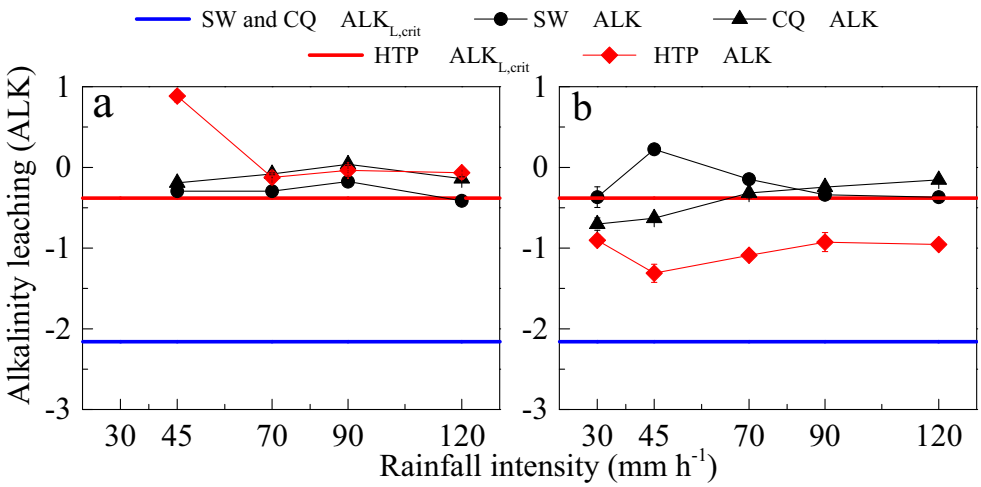

Fig. 7 Alkalinity leaching (keq ha^{-1} a^{-1}) in **a** surface flow and **b** subsurface flow in SW, CQ, and HTP under the different rainfall intensity treatments

on the soil surface (Xin et al. 2008; Yi et al. 2012; Hao et al. 2018). When rainfall intensity is lower than the soil infiltration rate, all precipitation is converted into subsurface flow, and surface flow does not occur. When rainfall intensity exceeds the soil infiltration rate, rainwater quickly joins to form surface flow on the soil surface (Dai et al. 2015; Liu et al. 2014). In this study, 45 mm h^{-1} is the critical rainfall intensity threshold of surface flow in the study area. As rainfall intensity continued to increase, the rainwater collection rate increased, and the initial runoff yield time decreased (Xin et al. 2008; Zhang and Zheng 2011). Furthermore, the infiltration rate of different soils is affected by soil physical properties; therefore, under simulated rainfall treatments, runoff characteristics of the three lithologic soil formations employed in this study varied widely under the rainfall intensity treatments investigated.

Migration characteristics of base cations

When the rain intensity and rainfall are heavier, the underground network in the karst area provides a preferential flow pathway for the rapid loss of water and nutrients, while in the nonkarst area, due to the absence of underground passage, the rainwater can only enter the soil slowly in the form of infiltration. With the increase of rain intensity, a large amount of rainwater is collected into surface flow and loss; thus, the proportions of water and base cations in subsurface flow decrease. This phenomenon confirms that the developed underground structure in the karst area is one of the important factors leading to water and nutrient loss.

Soils in SW were mainly formed by carbonate mineral weathering, and the bedrock, dolomite (chemical formula $CaMg(CO_3)_2$), provided abundant Ca^{2+} and Mg^{2+} for the soil (Jiang 1999). Runoff increased with an increase in rainfall intensity, and Ca^{2+} and Mg^{2+} ions continuously dissolved in rainwater, resulting in an increase in Ca^{2+} and Mg^{2+} loss loads in surface flow and subsurface flow. In the CQ area, the bedrock was limestone (chemical formula $CaCO_3$) and there were a lot of Ca^{2+}in the soil, and the loss load of Ca^{2+} in subsurface flow in CQ was much higher than that in the other two sites. In the HTP area (nonkarst), due to the slow infiltration velocity of the rainwater to the soil and the less infiltration of water, Ca^{2+} and Mg^{2+} loss loads in subsurface flow were less affected by the rain intensity.

In the simulated rainfall experiment in the laboratory (Peng et al. 2017), there was no significant correlation between TK concentration and rainfall intensity. Our experiments found that losses in [K^+] and [Na^+] were negatively correlated with rainfall intensity, with loss values in the order of 45 > 70 > 90 > 120 mm h^{-1}, which probably means that there was a lot of mineral potassium in the runoff with an increase in rainfall intensity.

Besides, K^+ and Na^+ are highly soluble elements and liable for loss, and even when rainfall intensity is low, the concentrations in runoff or leachate could be very large. When rainfall intensity is higher, the volume of runoff is larger and it will lead to the dilution effect of K^+ and Na^+, resulting in lower [K^+] and [Na^+] with larger rainfall intensity. On the other hand, the rainfall's dilution effect to Ca^{2+} and Mg^{2+} is not so obvious. Statistical analysis shows that there were significant positive correlations between [Ca^{2+}] and [Mg^{2+}] and rainfall intensity in general, and Ca^{2+} and Mg^{2+} loads increased rapidly with an increase in rainfall intensity in SW and CQ areas (Table 4) which indicated that the bedrock in the karst area was easy to dissolve and be eroded, and the dissolution of dolomite and limestone produced a large amount of Ca^{2+} and Mg^{2+} ions. In addition, because of the high Mg^{2+} content in dolomite (Jiang 1999; Wang et al. 2016), losses in Mg^{2+} concentrations and loads in surface flow and subsurface flow in lime soil that developed from dolomite weathering were significantly higher compared to the other two types of soil investigated.

Losses in K^+ and Na^+ loads from subsurface flow were higher compared to those from surface flow in SW and CQ. Results showed that losses in K^+ and Na^+ resulting from

rainwater in dolomite and limestone soil formations were primarily through subsurface flow. Mass losses in K^+ in the karst areas caused by rainfall can cause plant growth retardation and leaf tissue necrosis in acute shortage (Zörb et al. 2014). Salinization is caused by large Na^+ leaching in downstream water and soil and causes salt damage in plants (Sun et al. 2015; Zhang et al. 2014b).

Maximum loss loads for all base ions investigated occurred under the higher rainfall intensity treatments (90 or 120 mm h^{-1}). The maximum loss load of Ca^{2+} was 32.86 kg ha^{-1}, and the maximum loss load of Mg^{2+} was 19.84 kg ha^{-1}. Significant losses in Ca^{2+} and Mg^{2+} ions not only lead to soil nutrient imbalance and leanness which promotes the rocky desertification in karst areas but can also cause overly high surface and groundwater hardness (Cardona et al. 2004; Elhatip et al. 2003; Jalali 2007), downstream river and reservoir pollution, and ecological environment deterioration.

In the karst area, more than 80% of the base cation loss load occurred in the limestone karst area. Losses of base cations and water through the subsurface flow were more than half of total loss, and in the limestone karst area, that proportion was more than 80%. Therefore, it is crucial in maintaining the stability of regional ecological system to reduce nutrients and moisture losses in subsurface flow in karst area, especially the limestone karst area. The phenomenon of rock dissolution and erosion in the karst area should not be neglected, and we can consider to increase the vegetation cover area and enhance the canopy interception of rainfall by plants to reduce erosion of bedrock by rainfall.

Alkalinity leaching in different lithologic soil formations

Alkalinity is one of the important properties of soils (Duan et al. 2000). If the value of alkalinity leaching from soil becomes greater, the change buffering capacity of soil for acid will be more weakened which may affect the stability of ecosystems. Alkalinity leaching values in surface flow and subsurface flow in both karst and nonkarst areas had no significant difference under the different rainfall intensities, but the path of alkalinity leaching was different between the karst area and nonkarst area. Alkalinity leaching in subsurface flow in the karst area was greater than that in the nonkarst, while the values of alkalinity leaching in subsurface flow were close in both areas. The developed underground structure in the karst area will lead to more alkalinity leaching, and the risk of soil acidification is greater. Therefore, in order to protect the fragile ecological environment in the karst area and avoid the risk of soil acidification due to loss of alkalinity, we should consider the change of land uses in the karst area to reduce the influence of excessive leaching of alkalinity.

Studies have shown that surface litter cover (Xu and Long 2005; Xue et al. 2010) is effective in absorbing precipitation, reducing runoff and soil nutrient losses in surface and subsurface flow (Carroll et al. 2000) and reducing alkalinity leaching and therefore reducing the risk of soil acidification. Vegetation plays a major role in reducing the impact of rain on soil erosion, and it also greatly improves surface litter cover. Therefore, afforestation and vegetation cover expansion in karst areas can effectively reduce losses in soil base cations and alkalinity leaching, which could ultimately prevent rocky desertification and acidification from occurring (Song et al. 2014).

Conclusions

In the present study, subsurface flow is the dominant channel for the loss of water and base cations in the karst area, especially under small rainfall intensity, and the developed underground structure will lead to more alkalinity leaching and greater risk of soil acidification. To reduce nutrient and moisture losses in subsurface flow in the karst area and erosion of bedrock by rainfall, it is necessary to consider to increase the vegetation cover area and enhance the canopy interception of rainfall by plants. In addition, surface litter cover is effective in absorbing precipitation, which can buffer the erosion effects of rain on soil and reduce soil nutrient losses and alkalinity leaching. Therefore, afforestation would be an effective means in preventing soil rocky desertification and acidification in karst areas.

Acknowledgments The authors of this study would like to thank all anonymous reviewers for their helpful remarks.

Funding information This study was financially supported by the National Nature Science Foundation of China (Nos. 41571130043 and 31570465) and the Youth Innovation Promotion Association of the Chinese Academy of Sciences.

References

Cai YL (1996) Preliminary research on ecological reconstruction in karst mountain poverty areas of southwest China. Adv Earth Sci 11:602–606

Cardona A, Carrillorivera JJ, Huizarálvarez R, Granielcastro E (2004) Salinization in coastal aquifers of arid zones: an example from Santo Domingo, Baja California Sur, Mexico. Environ Geol 45:350–366

Carroll C, Merton L, Burger P, Loch R, Jasper D (2000) Impact of vegetative cover and slope on runoff, erosion, and water quality for field plots on a range of soil and spoil materials on central Queensland coal mines. Aust J Soil Res 38:313–328

Chen H, Nie Y, Wang K (2013) Spatio-temporal heterogeneity of water and plant adaptation mechanisms in karst regions: a review. Acta Ecol Sin 33:317–326

Cheng L, Zhu J, Chen G, Zheng X, Oh NH, Rufty TW, Richter DDB, Hu S (2010) Atmospheric CO2 enrichment facilitates cation release from soil. Ecol Lett 13:284–291

Cronan CS, Grigal DF (1995) Use of calcium/aluminum ratios as indicators of stress in forest ecosystems. J Environ Qual 24:209–226

Dai Q, Liu Z, Shao H, Yang Z (2015) Karst bare slope soil erosion and soil quality: a simulation case study. Solid Earth 6(3):985–995

Duan L, Hao JM, Alan J, Rob C, Chris E, Xie SD (2000) Mapping critical loads of acid deposition for soils in China. Tsinghua Sci Technol International Journal on Information Science 5:270–278

Duan L, Hao JM, Xie SD, Zhou Z (2002) Estimating critical loads of sulfur and nitrogen for Chinese soils by steady state method. Chinese J Environ Sci-China 23:7

Elhatip H, Afşin M, Kuşçu L, Dirik K, Kurmaç Y, Kavurmacı M (2003) Influences of human activities and agriculture on groundwater quality of Kayseri-Incesu-Dokuzpınar springs, central Anatolian part of Turkey. Environ Geol 44:490–494

Gattward JN, Almeida AAF, Souza JO, Gomes FP, Kronzucker HJ (2012) Sodium–potassium synergism in Theobroma cacao: stimulation of photosynthesis, water-use efficiency and mineral nutrition. Physiol Plant 146:350–362

Hao Z, Gao Y, Sun XM, Wen XF (2018) Differential isotopic characteristics of eco-hydrologic processes in a subtropical watershed, China. Ecohydrology:e1944

Huang SS, Ye C, Zhong YJ, Cheng YH, Wu L, Huang QR, Zheng W, Sun YM, Zhang K, Zhang XL (2016) Soil cation exchange capacity and exchangeable base cations as affected by land use pattern in sloping farmland of red soil. Soil Crop 5:72–77

Jalali M (2007) Hydrochemical identification of groundwater resources and their changes under the impacts of human activity in the Chah basin in western Iran. Environ Monit Assess 130:347–364

Jiang ZC (1999) Element migration of Karst dynamic system. Acta Geograph Sin 54(5):438–444

Liang WJ, Wang ML, Ai XZ (2009) The role of calcium in regulating photosynthesis and related physiological indexes of cucumber seedlings under low light intensity and suboptimal temperature stress. Sci Hortic 123:34–38

Liu L, Zhou YY, Song CY, Li FS (2008) Release of basic cations in red soil under simulated acid rain and buffering mechanism. Res Environ Sci 21:49–55

Liu ZT, Dai QH, Yang Z (2014) Study of simulated soil erosion on a bare karst slope. Carsologica Sinica 33(03):356–362

Lucas RW, Klaminder J, Futter MN, Bishop KH, Egnell G, Laudon H, Högberg P (2011) A meta-analysis of the effects of nitrogen additions on base cations: implications for plants, soils, and streams. For Ecol Manag 262:95–104

Peng X, Dai Q, Li C, Yuan Y, Zhao L (2017) Effect of simulated rainfall intensities and underground pore fissure degrees on soil nutrient loss from slope farmlands in karst region. Trans Chin Soc Agric Eng 33: 131–140

Pettigrew WT (2008) Potassium influences on yield and quality production for maize, wheat, soybean and cotton. Physiol Plant 133:670–681

Powers JS, Salute S (2011) Macro- and micronutrient effects on decomposition of leaf litter from two tropical tree species: inferences from a short-term laboratory incubation. Plant Soil 346:245–257

Qian J, Zhang LP, Wang WY, Liu Q (2014) Effects of vegetation cover and slope length on nitrogen and phosphorus loss from a sloping land under simulated rainfall. Pol J Environ Stud 23:835–843

Silva LVF, Golombieski JI, Baldisserotto B (2003) Incubation of silver catfish, Rhamdia quelen (Pimelodidae), eggs at different calcium and magnesium concentrations. Aquaculture 228:279–287

Song T, Peng W, Du H, Wang K, Zeng F (2014) Occurrence, spatial-temporal dynamics and regulation strategies of karst rocky desertification in southwest China. Acta Ecol Sin 12:131–140

Song XW, Gao Y, Wen XF, Guo DL, Yu GR, He NP, Zhang JZ (2017a) Carbon sequestration potential and its eco-service function in the karst area, China. J Geogr Sci 27(8):967–980

Song XW, Gao Y, Green SM, Dungait JAJ, Peng T, Quine TA, Xiong BL, Wen XF, He NP (2017b) Nitrogen loss from karst area in China in recent 50 years: an in-situ simulated rainfall experiment's assessment. Ecol Evol 7(23):10131–10142

Sun C, Gao X, Fu J, Zhou J, Wu X (2015) Metabolic response of maize (Zea mays L.) plants to combined drought and salt stress. Plant Soil 388:99–117

Sverdrup H, Vries WD (1994) Calculating critical loads for acidity with the simple mass balance method. Water Air Soil Pollut 72:143–162

Sweeting MM. 1993. Reflections on the development of karst geomorphology in Europe and a comparison with its development in China. 37:127–136

Tang XF, Wang YQ, Wang YJ, Guo P, Hu B, Sun SQ (2014) Influence of hydrological processes on the runoff variation of base cations in Jinyun Mountain. Acta Ecol Sin 34:7047–7056

Tuyet D (2001) Characteristics of karst ecosystems of Vietnam and their vulnerability to human impact. Acta Geol Sin-Engl Edition 75:325–329

Wang W, Dai W (2012) Study on soil pH and acidic buffering properties in Anhui Province. Chin Agric Sci Bull 15:017

Wang ML, Zhang (2010) Effects of Ca2+ and Mg2+ concentrations on growth, SOD and CAT enzymatic activity of juvenile Paralichthys olivaceus. Prog Fish Sci 31:29–36

Wang S, Wan C, Wang Y, Chen H, Zhou Z, Fu H, Sosebee RE (2004) The characteristics of Na+, K+ and free proline distribution in several drought-resistant plants of the Alxa Desert, China. J Arid Environ 56:525–539

Wang LC, Hu WX, Wang XL, Cao J, Wu HG, Liao ZW, Wan Y (2016) Variation of Sr content and ~(87)Sr/~(86)Sr isotope fractionation during dolomitization and their implications. Oil Gas Geol 37:464–472

Watmough SA, Dillon PJ (2004) Major element fluxes from a coniferous catchment in central Ontario, 1983-1999. Biogeochemistry 67:369–399

Xiao H, Weng Q (2007) The impact of land use and land cover changes on land surface temperature in a karst area of China. J Environ Manag 85:245–257

Xin W, Zhu B, Tang JL, Luo ZX, Liu YJ, Shi DM (2008) Simulation study of characteristics of runoff and sediment yield in the hill area with purple soils. Bull Soil Water Conserv 28:31–35

Xu Y, Long J (2005) Effect of soil physical properties on soil erosion in Guizhou karst mountainous region. J Soil Water Conserv 1:39

Xu ZW, Jiang Y, Zhang YG, Jiang DM (2013) Soil exchangeable base cations along a chronosequence of Caragana microphylla plantation in a semi-arid sandy land, China. J Arid Land 5:42–50

Xue L, Fu JD, Zheng WG, Zhao HJ, Tan JD, Zhang XP (2010) Effect of litterfall cover on runoff and potassium loss in Pinus caribaea stands. For Res 23:510–514

Yang Z, Dai QH, Huang QH, Wu XQ (2010) Experimental study of runoff processes on typical karst slope. J Soil Water Conserv 24:78–81

Yi H, Dai QH, Wang PJ (2012) Runoff features and the influencing factors on karst sloping farmland. J Soil Water Conserv 26:46–51

Yuan DX 1997 Rock desertification in the subtropical karst of south China. Z Geomorphol 108:81–90

Zhang HR, Zheng FL (2011) Effect of slope gradients on erosion from a red soil hillslope under different rainfall intensity. J Soil Water Conserv 25:40–43

Zhang D, Shi W, Zhou D, Li R (2001) Intrinsic driving mechanism of land rocky desertification in karst regions of Guizhou province. Bull Soil Water Conserv 21:1–5

Zhang W, Wang B, Yang G, Zhang K (2014a) Erosive rainfall and characteristics analysis of sediment yield on yellow soil area in karst mountainous. Ecol Environ Sci 23:1776–1782

Zhang X, Lu G, Long W, Zou X, Li F, Nishio T (2014b) Recent progress in drought and salt tolerance studies in Brassica crops. Breed Sci 64: 60–73

Zheng X, Chen X, Zhang ZC (2014) Rainfall-runoff response characteristic analysis of Chenqi karst watershed in southern China. Earth Environ 42:000221–000227

Zörb C, Senbayram M, Peiter E (2014) Potassium in agriculture—status and perspectives. J Plant Physiol 171:656–669